Available online at www.sciencedirect.com
ScienceDirect
Ceramics International 37 (2011) 1775–1780
CERAMICS INTERNATIONAL
www.elsevier.com/locate/ceramint

Synthesis, microstructure, and photocatalysis of In_2O_3 hollow particles

Tzu-Tsung Tseng, Jun-Yen Uan, Wenjea J. Tseng *

Department of Materials Science and Engineering, National Chung Hsing University, 250 Kuo Kuang Road, Taichung 402, Taiwan

Received 13 December 2010; received in revised form 4 January 2011; accepted 27 January 2011
Available online 29 March 2011

Abstract

Indium oxide (In_2O_3) microspheres with hollow interiors have been prepared by a facile implantation route which enables indium ions released from indium-chloride precursors to implant into nonporous polymeric templates in C_2Cl_4 solvent. The templates are then removed upon calcination at 500 °C in air atmosphere, forming hollow In_2O_3 particles. Specific surface area (0.5–260 $m^2\ g^{-1}$) and differential pore volume (7×10^{-9} to $3.8 \times 10^{-4}\ m^3\ g^{-1}\ Å^{-1}$) of the hollow particles can be tailored by adjusting the precursor concentration. For the hollow In_2O_3 particles with high surface area (260 $m^2\ g^{-1}$), an enhanced photocatalytic efficiency (up to ~one-fold increase) against methylene blue (MB) dye is obtained under UV exposure for the aqueous In_2O_3 colloids with a dilute solids concentration of 0.02 wt.%.

Keywords: Indium oxide; In_2O_3; Template synthesis; Hollow particle; Photocatalysis

1. Introduction

Semiconductive indium oxide (In_2O_3) with a wide bandgap (direct bandgap around 3.6 eV at room temperature) has attracted much attention in recent years, owing mainly to its potential applications in solar cell [1], field-emission display [2], lithium-ion battery [3], biosensor [4], gas sensor [5–7], optoelectronics [8], and photocatalysis. Nanostructured In_2O_3 hollow particles with tailored morphology and surface functionality, in particular, present unique properties that may respond quickly to minute changes from specific external stimuli, giving rise to a selective sensing capability and possibly a prolonged device life-time [9–16].

Many methods have been employed to prepare inorganic hollow spheres [17], including template-directed [10–12,18] and template-free methods [9,13–16]. For the template-directed synthesis, hard templates (such as polystyrene latex particles, colloidal silica sols, and carbon particles) or soft templates (such as micelles, vesicles, and microemulsion droplets) are used in a way that preferential adsorption or uniform coating of shell materials occurs on the surface of template cores [17]. A pioneering layer-by-layer (LbL) synthesis scheme proposed by Caruso et al., for example, demonstrated that addition of shell layers or precursor materials can be deposited sequentially on the template surface via alternate adsorption of oppositely charged species [18]. By this means, hollow In_2O_3 particles with nanoporous shells were prepared from hydrolysis of $InCl_3$ using carbonaceous spheres as the sacrificial templates [10]. Similarly, Xu et al. used sulfonated polystyrene particles as a template for synthesis of tin-doped In_2O_3 hollow particles [11]. The LbL method is general (i.e., applicable to a wide range of different materials) but is tedious in practice. In addition, functionalization of the template surface is often required to ensure the formation of uniform shell. In this regard, porous colloidal particles (such as mesoporous polymeric beads) were alternatively used as a template for the synthesis of hollow In_2O_3 particles [12]. The advantage of using such porous templates is that the precursors or nanoparticles can be infiltrated into the porous channel within the templates, leading to formation of discrete, non-aggregating In_2O_3 particles with a narrow particle-size distribution after template removal. The infiltration scheme is yet difficult to control, i.e., hollow In_2O_3 particles with various shell thicknesses are often formed, resulted in a high fraction of broken spheres since that an insufficient robustness of the shell might occur upon the template-removal step.

Herein, we report a facile one-step synthesis route for the preparation of discrete hollow In_2O_3 spheres with a uniform shell thickness. The process used nonporous polydivinylbenzene spheres as a template, and is featured with an

* Corresponding author. Tel.: +886 4 2287 0720; fax: +886 4 2285 7017.
E-mail address: wenjea@dragon.nchu.edu.tw (W.J. Tseng).

0272-8842/$36.00
doi:10.1016/j.ceramint.2011.01.046

''implantation'' of indium ions from the precursors into the template surface [19]. In addition, the process requires no need for prior modifications on the template surface. Microstructure and photocatalytic property of the hollow In_2O_3 particles were examined as the precursor concentration varies.

2. Experimental procedure

2.1. Synthesis

Anhydrous indium chloride ($InCl_3$, Alfa, 99.99%, U.S.A.) was used as the precursor. Analytical-grade tetrachloroethylene (C_2Cl_4, Aldrich, U.S.A.) was used as received without further purification as a solvent. The $InCl_3$ of 0.01–0.15 g was first mixed with the C_2Cl_4 solvent (10 ml) at a reaction temperature of 75 °C, before addition of 0.25 g polymeric beads (which are divinyl benzene cross-linked with resin, and are of 3 μm in diameter, Sekisui, Japan) as the colloidal template. The solutions were then continuously agitated for an additional isothermal holding of 5 h at 75 °C, followed by repeated centrifuging and washing of the template particles by mild HCl solution (5 wt.%) and acetone, respectively. The particles were then dried in an oven at 60 °C, and were heated to 600 °C in a tube furnace to burn out the polymeric cores.

2.2. Characterization

Elemental distribution of the oven-dried particles was examined by field-emission electron spectroscopy for chemical analysis (ESCA, PHI 5000 Versa Probe/Scanning ESCA Microprobe, ULVAC-PHI, Japan) equipped with a C_{60} ion gun for the elemental depth-profiling analysis. The particles were first uniformly dispersed in ethanol via an ultrasonic agitation (Sonicator 3000, Misonix, U.S.A.). A few drops of the powdered dispersions were then placed onto an electrically conductive glass plate by a pipette before being dried again ready for the analysis [19]. A scanning area of approximately 400 μm^2 was carried out on the particle assemblies with an increasing energy increment of 0.1 eV per step (equivalent to nominally 1.73 nm per step in vertical direction). A total of 20 etching steps were performed, which corresponds to a nominal penetration depth of up to 34.5 nm from the top surface of the powdered assemblies first bombarded by the focused electron beam. Peak intensities from In(5d) and O(1s) were collected and compared over the penetration-depth range examined.

About 1 ml of the solutions consisting of the $InCl_3$ precursor of 0.15 g after the isothermal reaction (75 °C for 5 h) was diluted in two steps with de-ionized water (18.2 MΩ, Millipore, U.S.A.) in a weight ratio of 1:100. Upon completion of the first dilution step, the water–solvent mixture was allowed to settle without disturbance. Only part of the liquid from the water portion was taken out by a pipette for further dilution in water. The diluted aqueous solution was then injected into a sample loop of ion chromatography (IC, ICS-900, Dionex, U.S.A.). The solution was carried onto a stationary column that contains an ion-exchange resin with covalently bonded charged functional groups. Targeted analyte molecules, i.e., Cl^- anions (if any) from the dissolution of $InCl_3$ in the C_2Cl_4 solvent, were retained on the stationary phase by Coulombic interactions but were allowed to be eluted by increasing the concentration of a similarly charged species, i.e., aqueous solution consisting of sodium hydrogen carbonate (($NaHCO_3$) as an eluent) that displaces the Cl^- anions from the stationary phase. The elapsed time required for the ions to desorb from the stationary resin was determined by conductivity measurement and compared with standards for qualitative and quantitative measures. For comparison reasons, reaction solutions without the addition of $InCl_3$ precursor but have gone through the entire reaction process (75 °C for 5 h) were also prepared and tested by IC in order to verify that the Cl^- anions indeed came from the dissolution of precursor, not from the hydrolysis of C_2Cl_4 solvent in water.

Thermogravimetric and differential thermal analyses (TG/DTA, Diamond 6300, Perkin Elmer, U.S.A.) were used to examine the decomposition of the polymeric cores at elevated temperatures. The samples were heated to 600 °C at a constant heating rate of 10 °C min^{-1} in flowing air. Pore structure and surface area of the hollow In_2O_3 particles were determined from nitrogen gas adsorption–desorption (ASAP 2020, Micromeritics, U.S.A.) at the boiling point of liquid nitrogen (77.4 K). Particle-size distribution was measured by a dynamic light-scattering technique (DLS, Nano ZS, Malvern, U.K.). X-ray diffraction (XRD) analysis was performed using a Mac Science X-ray diffractometer (MXP-III, Japan) with a CuKα radiation (λ = 1.5406 Å). Bandgap energy of the hollow In_2O_3 particles was determined from the optical absorption by UV–vis spectrophotometry equipped with an integrated sphere (Lambda 800, Perkin Elmer, U.S.A.). Surface morphology and hollow structure of the In_2O_3 spheres were examined by field-emission scanning electron microscopy (FE-SEM, JSM 6700F, JEOL, Japan) and transmission electron microscopy (TEM, JEM-1200CXII, JEOL, Japan), respectively.

2.3. Photocatalytic activity

Photocatalytic experiment was conducted in aqueous solutions with UV irradiation (200 W mercury lamp) up to 90 min; to which, addition of the In_2O_3 hollow particles in the solutions was held at 0.2 g L^{-1} and the initial methylene blue (MB) concentration was at 5×10^{-6} M. Prior the test, all the solutions were kept in darkness for 10 min to establish an adsorption–desorption equilibrium. Some samples were siphoned out from the reaction solutions after different UV-exposure times and then quickly centrifuged to separate the particles from the solutions. The clear solutions were then immediately characterized by the UV–vis spectrophotometry to determine the absorption change over a range of wavelengths from 200 to 900 nm. Residual MB concentration was determined from the absorption change using a 5-point calibration curve.

3. Results and discussion

The as-received polymer beads showed a Brunauer–Emmett–Teller (B.E.T.) surface area of 5.9 m^2 g^{-1} from the nitrogen gas adsorption–desorption measurement. Differential

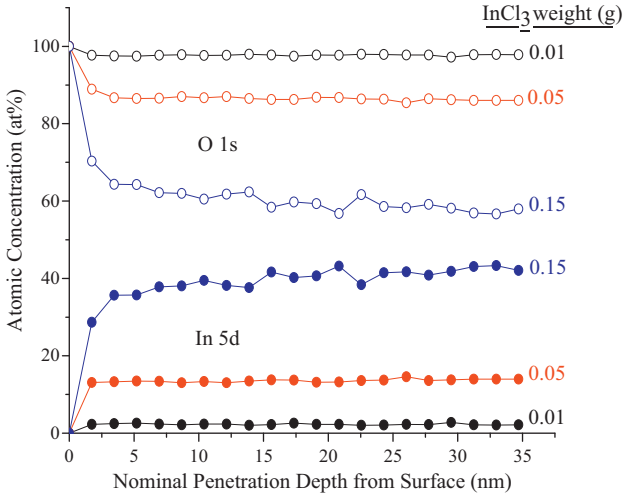

Fig. 1. Elemental distribution of In(5d) and O(1s) in depth-profiling ESCA analyses for the reacted core–shell particles prepared under various $InCl_3$ concentrations.

pore volume was barely minimal, i.e., less than 2.5×10^{-11} m^3 g^{-1} $Å^{-1}$ over a broad range of pore diameter (up to 1600 Å from 17 Å) by the Barrett–Joyner–Halenda (B.J.H.) method, revealing that the polymeric beads used for the template core were essentially nonporous. Fig. 1 shows the elemental depth profile from the ESCA analyses. The intensities of In(5d) and O(1s) peaks originate from the indium precursor and the polymeric template, respectively. A predominance of In(5d) at the surface with a decreasing concentration toward the inner core is expected if the indium precursors were coated on the template particles. Fig. 1 shows just the opposite; to which, a decreasing O(1s) intensity along with a conjugating increase of the In(5d) peak intensity occurs at the shallow penetration region, providing a direct evidence that the indium species tend to reside underneath the surface of the nonporous templates in the given solvent to form a core–shell structured composite particles with an outer diameter no greater than their as-received counterparts (SEM not shown here). In addition, the indium concentration becomes more pronounced as the precursor concentration was increased. This indicates that more indium was made possible to implant underneath the template surface. The concentration profiles of indium yet all appear to reach a plateau before getting to a nominal penetration depth of ca. 3 nm. Since the scanning area of the ESCA analyses ($\sim$400 μm^2) covered indeed over hundreds of the particles in the powdered assemblies, the saturation in concentration is suspected to be ascribed to the various protruding heights of the powders over the relatively broad scanning area examined [19]. A separate experiment by using template particles of the same composition but of a much greater particle diameter (500 μm) and with the use of platinum chloride as a precursor has been conducted with an aim that the depth-profiling ESCA measurement can be performed on single template particle alone [20]. The analyses showed that concentration of platinum metal reached a maximum at a similar penetration depth of 5 nm, and the concentration began to decrease as the penetrating depth was further increased.

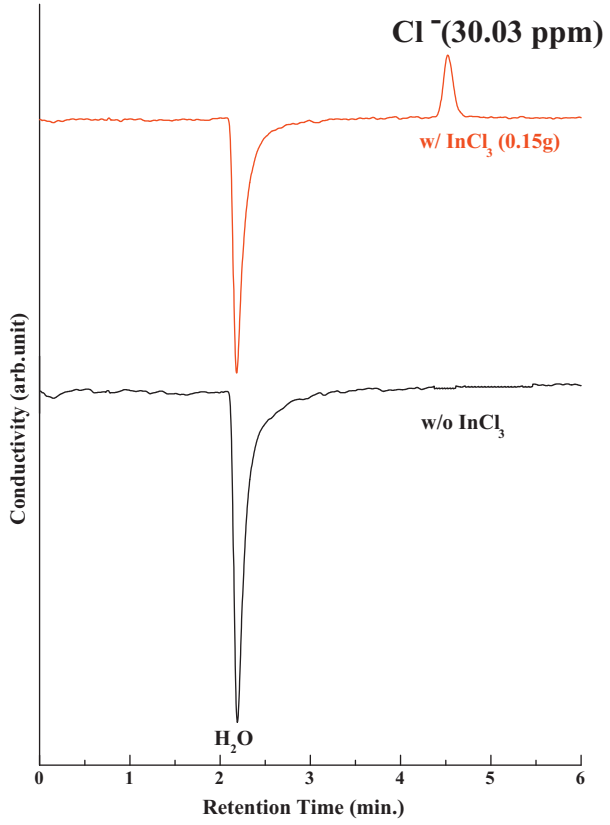

Fig. 2. Electrical conductivity vs. retention time from ion chromatography.

When the polymeric beads of 3 μm diameter were used, an identical trend with the saturation as that of Fig. 1 was resulted for the platinum distribution. This finding supports our hypothesis about the cause for the observed saturation plateau in the indium concentration profiles. Nonetheless, the implanted indium concentration increases apparently with the precursor concentration (Fig. 1), the "effective" implantation depth appears to remain virtually the same over a shallow distance (< ca. 5 nm) from the surface, regardless of the various precursor concentrations used.

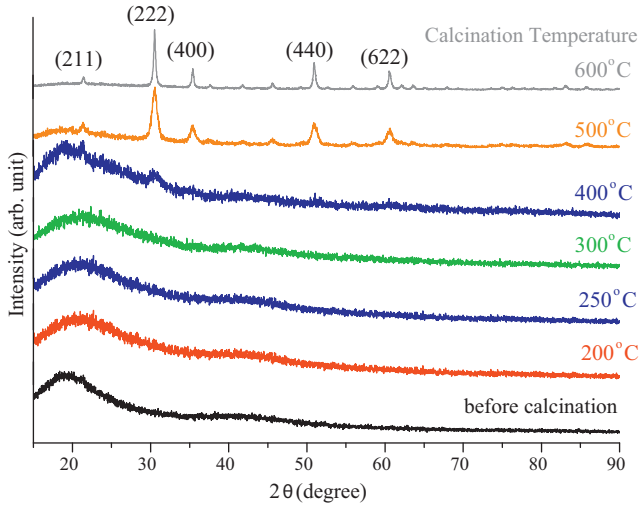

Fig. 3. XRD patterns of In_2O_3 hollow particles calcined at different temperatures.

Fig. 2 shows the conductivities over a range of retention times in the IC measurement. For the diluted solutions without the addition of $InCl_3$ precursor but have being through the entire reaction process, only a peak ascribing to water (at a retention time just slightly beyond 2 min) was found. In comparison, an additional peak belonging to the Cl^- anions (at a retention time of 4.6 min) was apparent as $InCl_3$ precursor was introduced into the reaction. This indicates that the dissolution of $InCl_3$ into In^{3+} and Cl^- ions occurred in C_2Cl_4 solvent, suggesting that the implanted indium species underneath the template surface were most likely of the In^{3+} ions. In fact, this finding is in parallel with our earlier findings from solid-state ^{27}Al nuclear magnetic resonance (NMR) spectroscopy [19,21]; to which, Al^{3+} ions preferred to bond with O^{2-} ions in the polymeric templates to form the shell layer.

Upon exposure to elevated temperatures, the polymeric template began to decompose at temperatures above 250 °C in air atmosphere, and was completely removed by 500 °C from the TG/DTA measurement [19]. In Fig. 3, XRD analysis reveals that the hollow spheres were amorphous in structure below 300 °C. At 400 °C, crystalline In_2O_3 began to form, which agrees quite well with our previous finding in preparing crystalline In_2O_3 via a hydrothermal route [22]. The degree of crystallinity of In_2O_3 phase appears to become more complete when the calcination temperature was raised above 500 °C. Microstructural observations reveal that the hollow In_2O_3

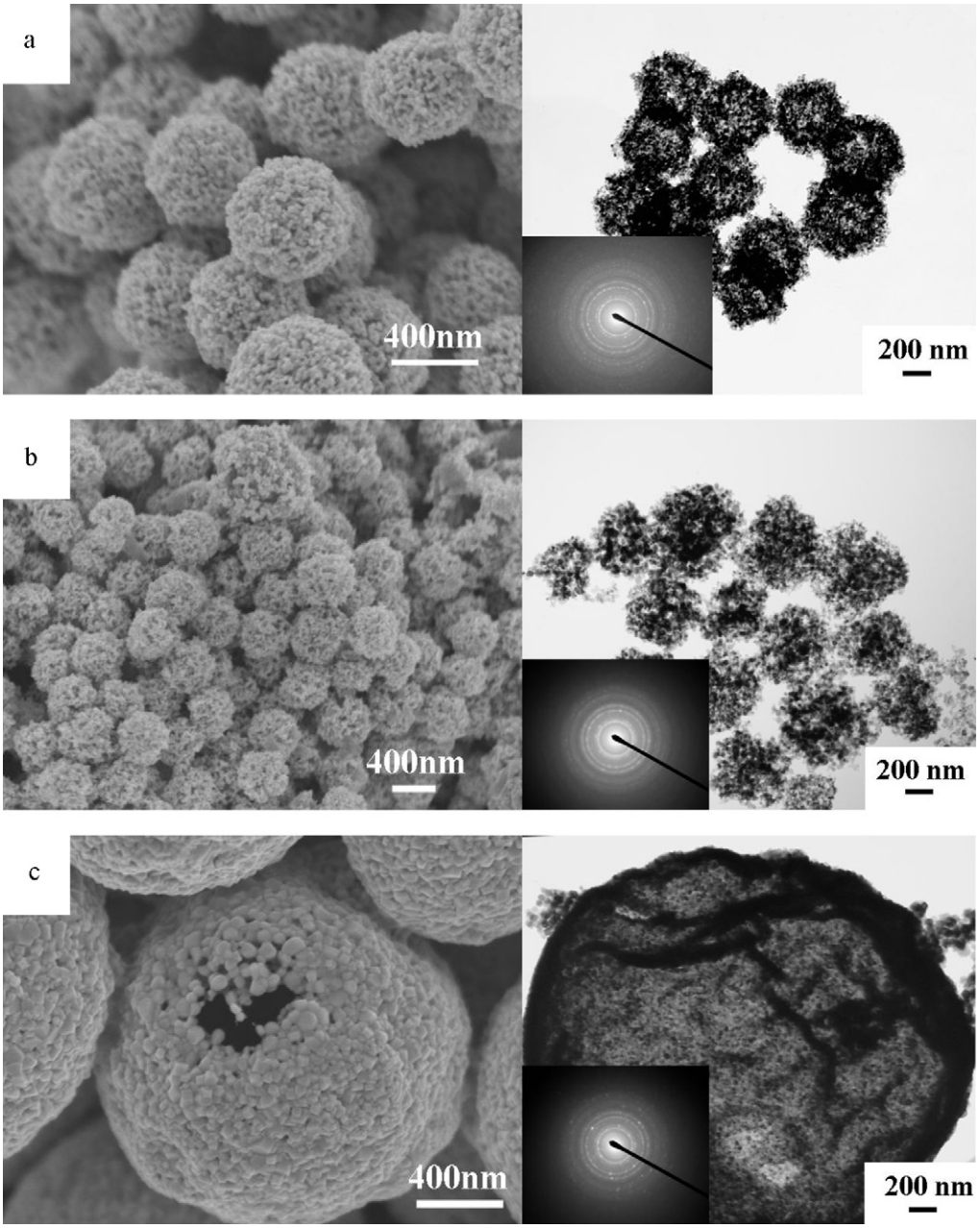

Fig. 4. Electron micrographs (Left: SEM, Right: TEM) of the In_2O_3 hollow particles prepared at various $InCl_3$ concentrations after 600 °C calcination. (a) $InCl_3$ 0.01 g, (b) $InCl_3$ 0.05 g, and (c) $InCl_3$ 0.15 g.

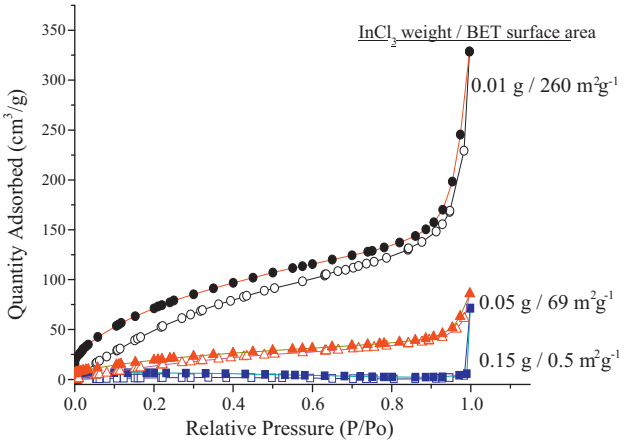

Fig. 5. The N_2 adsorption–desorption isotherms for the In_2O_3 hollow particles prepared from $InCl_3$ precursors of various concentrations.

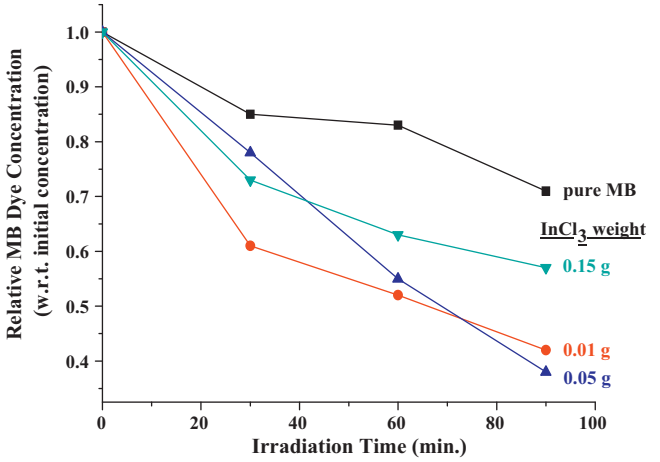

Fig. 6. Photodegradation of MB dye solutions under UV irradiation. The solids concentration of the hollow-particle suspensions was held at 0.02 wt.%.

particles were polycrystalline and consisted of many In_2O_3 crystallites as their building blocks for the shells (Fig. 4). The particle surface was rough; yet, the particles were essentially non-aggregating. Size of the hollow particles increased drastically as the precursor concentration reached 0.15 g. From the DLS measurement, all the hollow In_2O_3 particles presented a well-defined, unimodal particle-size distribution. The average particle sizes were 589, 710, and 1103 nm for the hollow particles prepared from $InCl_3$ concentrations of 0.01, 0.05, and 0.15 g, respectively. This finding agrees favorably with that of the ESCA analyses (Fig. 1) in a way that an increased indium concentration over the shallow region underneath the surface would lead to a more robust shell upon the organic pyrolysis step so that an increased particle size results. The shells were yet thin enough to allow the passage of the bombarded electron beams (in TEM case) even for the highest precursor concentration examined.

Fig. 5 shows the nitrogen adsorption–desorption behavior for the calcined, hollow In_2O_3 particles synthesized from the various precursor concentrations. The samples all showed a larger desorption volume than that of the adsorption ones over the pressure range examined, revealing that gas molecules were "trapped" within the interior chamber of the hollow particles because of fine pore channels of the shell. This hysteresis in gas adsoption–desorption appears to become more pronounced for the particles prepared from the 0.01 g $InCl_3$ concentration. The B.E.T. specific surface areas were 5, 69, 260 $m^2\ g^{-1}$ for the hollow particles from $InCl_3$ concentration of 0.15, 0.05, and 0.01, respectively. Pore size of the 0.01 g samples was of 2.5 nm, revealing a nanoporous shell structure. The differential pore volumes changed from 7×10^{-9}, 9×10^{-5}, to $3.8 \times 10^{-4}\ m^3\ g^{-1}\ Å^{-1}$ for the hollow particles prepared from the descending order of $InCl_3$ concentration. This indicates that the shell structure can be changed from nanoporous to a rather dense structure as the precursor concentration varies, revealing the capability of tailoring the shell structure for the implantation process.

Bandgap calculation from the UV–vis spectra indicates that the bandgap of the synthesized In_2O_3 hollow particles was 3.8 eV at room temperature, revealing the semiconductive nature. This together with the nanoporous shell structure (average pore size as small as 2.5 nm) and a B.E.T. specific surface area as high as 260 $m^2\ g^{-1}$ is considered beneficial to the photocatalytic performance. In Fig. 6, the concentration of aqueous MB dye solution generally reduces with the UV irradiation. The photocatalytic activity is yet enhanced pronouncedly by the presence of In_2O_3 hollow particles. The photodegradation of MB dye with an increased efficiency up to 121% was observed, i.e., relative MB concentration reduced from 72% of the pure MB case to a minimum of 38% for the suspensions containing the In_2O_3 hollow particles with the highest specific surface area. Note that the solids concentration was held constant and was of merely 0.02 wt.%. One might suspect that the improved photocatalysis stems primarily from the increase in adsorption of the MB dye molecules on the surface of In_2O_3 hollow particles, resulted in generation of the electron and hole pairs which serve as redox sites critically important to the photocatalytic activity when excited by the UV energy.

4. Conclusion

Non-agglomerating In_2O_3 hollow spheres with tailored shell structure have been prepared via a facile implantation route by the use of nonporous polymeric beads as a hard template. The implantation of indium ions has been verified by depth-profiling ESCA analysis; where the indium ions are embedded underneath the template surface in C_2Cl_4 solvent to form core–shell structure at the reaction temperature used. The penetration concentration increases pronouncedly as the precursor concentration increases; yet, the penetration depth appears to be independent of the precursor concentration. Instead of forming a coating layer on the template particles which might lead to particle aggregation upon the template removal, this implantation route allows for the formation of discrete particles with unimodal particle-size distribution. In addition, the shell structure can be tailored to a significant extent, i.e., changing from nanoporous to essentially dense, depending on the process variables such as precursor concentration. The In_2O_3 hollow

spheres are semiconductive. An enhanced photocatalytic activity has been observed in dilute hollow particle suspensions that may be ascribed to the increased adsorption of MB dye molecules in water.

Acknowledgment

Financial support from the National Science Council (Taiwan, R.O.C.) under contract no. NSC 95-2221-E-005-036-MY3 is gratefully acknowledged.

References

[1] Z.B. Zhou, R.Q. Cui, Q.J. Pang, Y.D. Wang, F.Y. Meng, T.T. Sun, Z.M. Ding, X.B. Yu, Preparation of indium tin oxide films and doped tin oxide films by an ultrasonic spray CVD process, Appl. Surf. Sci. 172 (2001) 245–252.
[2] Y.X. Liang, S.Q. Li, L. Nie, Y.G. Wang, T.H. Wang, In situ synthesis of In_2O_3 nanowires with different diameters from indium film, Appl. Phys. Lett. 88 (2006) 193119.
[3] D.W. Kim, I.S. Hwang, S.J. Kwon, H.Y. Kang, K.S. Park, Y.J. Choi, K.J. Choi, J.G. Park, Highly conductive coaxial SnO_2–In_2O_3 heterostructured nanowires for Li ion battery electrodes, Nano Lett. 7 (2007) 3041–3045.
[4] M. Curreli, C. Li, Y. Sun, B. Lei, M.A. Gundersen, M.E. Thompson, C. Zhou, Selective functionalization of In_2O_3 nanowire mat devices for biosensing applications, J. Am. Chem. Soc. 127 (2005) 6922–6923.
[5] S. Bianchi, E. Comini, M. Ferroni, G. Faglia, A. Vomiero, G. Sberveglieri, Indium oxide quasi-monodimensional low temperature gas sensor, Sens. Actuators B Chem. 118 (2006) 204–207.
[6] K.I. Choi, H.R. Kim, J.H. Lee, Enhanced CO sensing characteristics of hierarchical and hollow In_2O_3 microspheres, Sens. Actuators B Chem. 138 (2009) 497–503.
[7] J. Liu, T. Luo, F. Meng, K. Qian, Y. Wan, J. Liu, Porous hierarchical In_2O_3 micro-/nanostructures: preparation, formation mechanism, and their application in gas sensors for noxious volatile organic compound detection, J, Phys. Chem. C 114 (2010) 4887–4894.
[8] C.Y. Kuo, S.Y. Lu, T.Y. Wei, In_2O_3 nanorod formation induced by substrate structure, J. Cryst. Growth 285 (2005) 400–407.
[9] B. Li, Y. Xie, M. Jing, G. Rong, Y. Tang, G. Zhang, In_2O_3 hollow microspheres: synthesis from designed $In(OH)_3$ precursors and applications in gas sensors and photocatalysis, Langmuir 22 (2006) 9380–9385.
[10] Z. Guo, J. Liu, Y. Jia, X. Chen, F. Meng, M. Li, J. Liu, Template synthesis, organic gas-sensing and optical properties of hollow and porous In_2O_3 nanospheres, Nanotechnology 19 (2008) 345704.
[11] H. Xu, S. Ding, W. Wei, C. Zhang, X. Qu, J. Liu, Z. Yang, Template synthesis of tin-doped indium oxide (ITO) polymer and the corresponding carbon composite hollow colloids, Colloid. Polym. Sci. 285 (2007) 1101–1107.
[12] D.G. Shchukin, R.A. Caruso, Template synthesis and photocatalytic properties of porous metal oxide spheres formed by nanoparticle infiltration, Chem. Mater. 16 (2004) 2287–2292.
[13] A. Gurlo, G. Miehe, R. Riedel, Surfactant-free self-assembly route to hollow In_2O_3 microspheres, Chem. Commun. 19 (2009) 2747–2749.
[14] L.Y. Chen, Z.D. Zhang, Biomolecule-assisted synthesis of $In(OH)_3$ hollow spherical nanostructures constructed with well-aligned nanocubes and their conversion into C–In_2O_3, J. Phys. Chem. C 112 (2008) 18798–18803.
[15] H. Zhu, K. Yao, H. Zhang, D. Yang, InOOH hollow spheres synthesized by a simple hydrothermal reaction, J. Phys. Chem. B 109 (2005) 20676–20679.
[16] P. Zhao, T. Huang, K. Huang, Fabrication of indium sulfide hollow spheres and their conversion to indium oxide hollow spheres consisting of multipore nanoflakes, J. Phys. Chem. C 111 (2007) 12890–12897.
[17] X.W. Lou, L.A. Archer, Z. Yang, Hollow micro-/nanostructures: synthesis and applications, Adv. Mater. 20 (2008) 3987–4019.
[18] F. Caruso, R.A. Caruso, H. Möhwald, Production of hollow microspheres from nanostructured composite particles, Chem. Mater. 11 (1999) 3309–3314.
[19] Y. Wang, W.J. Tseng, A novel technique for synthesizing nanoshell hollow alumina particles, J. Am. Ceram. Soc. 92 (S1) (2009) S32–S37.
[20] W.T. Li, M.S. Thesis, National Chung Hsing University (2008).
[21] Y. Wang, M.S. Thesis, National Chung Hsing University (2007).
[22] T.T. Tseng, W.J. Tseng, Effect of polyvinylpyrrolidone on morphology and structure of In_2O_3 nanorods by hydrothermal synthesis, Ceram. Int. 35 (2009) 2837–2844.